IAC-14,B4,7B,5,x25554

SOLARA/SARA: FIRST STEPS TOWARD A SPACE-BASED RADIO INTERFEROMETRY CONSTELLATION

Mary Knapp
Massachusetts Institute of Technology (MIT), United States, mknapp@mit.edu

The Solar Observing Low-frequency Array for Radio Astronomy (SOLARA) and accompanying Separated Antennas Reconfigurable Array (SARA) communications system is a medium to long-term project being developed at MIT and JPL. SOLARA is a space-based sparse aperture radio telescope capable of aperture synthesis imaging in the spectral region between 100 kHz and 30 MHz. This spectral band is near or below the ionospheric cut-off, so astronomical signals in this range cannot be observed from the surface of the Earth. Interferometry is required to obtain reasonable angular resolution at long wavelengths, so SOLARA will be composed of multiple CubeSat-sized spacecraft flying in loose formation. Relaxed baseline measurement requirements at long wavelengths (cm to m) compared to higher frequency radio interferometry (micron to mm) or optical interferometry (nm) make this a tractable problem for CubeSats. Furthermore, tight formation flight is not required if baselines between spacecraft do not change significantly during integration times (seconds to minutes). SOLARA will focus primarily on observations of the sun and space weather as well as magnetospheric radio emission from the Earth and the giant planets, but it is intended as a pathfinder to a larger array capable of detecting exoplanetary radio emission.

This paper presents initial analysis of the mission concept as well as more detailed studies of the beam pattern of the interferometer. In addition to the system concept and radio science, this paper presents a path to the full constellation involving precursor missions to demonstrate key technologies for SOLARA/SARA. The first precursor mission will demonstrate an electric propulsion system which will be used for SOLARA's constellation management and attitude control. The second precursor mission is a Low-Earth orbit demonstration mission composed of two to four spacecraft. The second precursor mission will validate the radio science payload, intersatellite communication and correlation, and constellation maintenance control algorithms.

I. INTRODUCTION

Radio interferometry provides extremely high resolution and high sensitivity images of energetic cosmic phenomena as well as detailed maps of solar system planets and the sun. This powerful observational tool is limited at the lower end of the electro-magnetic spectrum by the plasma frequency of the F2 layer of the ionosphere and at the upper end by water absorption in the troposphere. This paper focuses on the use of a space-based constellation/formation of CubeSats to overcome the ionospheric low-frequency observational limit. By moving to space, interferometry below 10 MHz will be possible for the first time. There have been previous proposals for similar space-based low frequency arrays (ALFA [11], SIRA [12]), but these proposals were not successful due to high cost and complexity. The advent of CubeSats reduces cost due to standardized COTS components and plentiful launch opportunities and complexity because CubeSats naturally lend themselves to mass production. Current work in CubeSat-based low frequency arrays is being conducted by several groups [3], including the author's.

II. SCIENTIFIC MOTIVATION

The ultimate motivation for SOLARA is observation of radio emission from exoplanets. The scientific justification for observations of exoplanets in low frequency radio is provided below. Because even the nearest exoplanetary systems are parsecs away and any planetary radio signals are correspondingly weak, a constellation with the sensitivity to detect exoplanetary emission would require hundreds or possibly thousands of antennas to provide sufficient collecting area. SOLARA, with 10s of spacecraft, is itself a precursor mission (or seed) for this future constellation, although it will be highly capable for observations of the sun, solar system planets, and galactic/interstellar medium (ISM) observations. See [4] for details on the science

cases for galactic mapping, heliophysics, and solar system planets.

II.I. Exoplanet Observations

The exoplanet field has exploded since its birth in the early 1990s. Much of the work in the field has focused on detecting and characterizing exoplanets via optical or infrared observations. These techniques have proved extremely powerful and allow for the measurement of an exoplanet's mass, radius, orbit, and atmospheric composition. The density of an exoplanet can be calculated if both the mass (from radial velocity measurements) and the radius (from transit observations) are known. Knowing the density of an exoplanet gives some indication of the atmospheric and interior structure, but currently there is no direct observational probe into exoplanet interiors. Radio observations of exoplanets have the potential to provide such a probe by measuring the existence and strength of exoplanetary magnetic fields.

Soon after the detection of the first "hot Jupiter" exoplanets, radio astronomers began using ground-based instruments like the VLA to search for radio emission from these planets [5]. To date, however, no unequivocal detections of exoplanetary radio emission have been made [6]. There are several possible explanations for the lack of detections.

First, most studies have been carried out at 150 MHz or higher. Since the cut-off frequency for electron-cyclotron maser instability (CMI) emission scales with the magnetic moment of the planet [7], only planets with very strong magnetic moments would be detectable at these frequencies. As shown in **Error! Reference source not found.**, Jupiter, with the strongest magnetic moment of the solar system planets, has the highest cut-off frequency. Large low-frequency ground-based observatories like LOFAR and the LWA are now beginning to probe lower frequencies and may detect planets with magnetic moments comparable to Jupiter. However, four of the five solar system planets with strong magnetic moments (including the Earth) have cut-off frequencies that fall below the Earth's ionospheric cut-off, so they cannot be observed from the ground. The Earth's own auroral kilometric radiation (AKR) was discovered by spacecraft observations rather than ground-based observatories [8]. Exoplanets with similar magnetic moments to the solar system planets would also be undetectable from the Earth's surface.

Second, CMI radiation is typically beamed, so the Earth must be in the emission beam at the time of observation. Finally, planetary radio emission in our solar system is typically bursty with flux levels varying over several orders of magnitude on timescales of days to weeks.

II.II. Cyclotron Maser Instability (CMI) and Planetary Radio Emission

The radio end of the EM spectrum has been used very little for exoplanet detection/characterization until recently. Radio observations of solar system planets, however, led to the prediction of the existence and strength of Jupiter's magnetosphere long before any space missions measured Jupiter's magnetic field directly [9]. Magnetized planets and stars often emit radiation close to the electron gyrofrequency due to the cyclotron maser instability (CMI) [10]. For nonrelativistic electrons, the gyrofrequency is given by

$$\omega_{ce} = \frac{eB}{m_e} \quad (1)$$

where e is the electron charge, B is the magnetic field strength, and m_e is the electron mass. Radiation emitted via the CMI mechanism is highly circularly polarized, which makes it easily distinguishable from other sources. All of the planets in our solar system with strong magnetic fields (Earth, Jupiter, Saturn, Uranus, and Neptune) exhibit radio emission due to the CMI mechanism. This radiation is generally called auroral radio emission since the source region is the convergent field lines near the planet's magnetic poles. While the frequency of auroral radiation is governed by the field strength of the planet, the intensity of the radio signal is proportional to the intensity of the solar wind [11].

Jupiter's auroral emission was detected from the ground in the 1950s and a B-field strength of 7 Gauss was estimated [9]. No emission was detected from any other solar system planets at the time because their magnetic fields are weaker and the electron gyrofrequency is below the Earth's ionospheric cutoff. Typical plasma frequencies in the Earth's ionosphere are 1-10 MHz, so incoming EM radiation at or below those frequencies cannot

propagate through the ionosphere to telescopes on the ground [12].

Assuming that at least some exoplanets are similar to the planets in our solar system, some may have magnetic fields and emit auroral radio signals. Expected radio fluxes for exoplanets are expected to be roughly on the same order of magnitude as the host star's radio emission [13]. Jupiter's radio emission often outshines the sun. This is a major advantage compared to the ~10^{10} contrast ratio in the optical domain. Ground-based instruments have been searching for these expected radio signals for over a decade with little success. Given that only one of five planets in this solar system has auroral emission detectable from the Earth's surface, a plausible explanation for the non-detection of exoplanetary radio auroral emission is that exoplanetary field strengths are comparable to Solar System planets other than Jupiter and their auroral emission cutoff frequency is below the Earth's ionospheric cutoff. *A space-based observatory is necessary to search for emission from exoplanets with B-field strengths comparable to the Earth.*

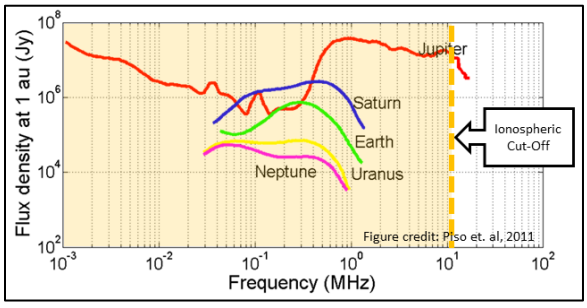

Figure 1 - Comparison of radio emissions from the strongly magnetized solar system planets.
Only Jupiter's radio emission is detectable from the Earth's surface. The dashed yellow line represents the ionospheric cutoff and the shaded region to the left of the line is inaccessible from the surface of the Earth.

III. SOLARA CONCEPT DESCRIPTION

SOLARA is a constellation mission composed of 16 CubeSat-class units deployed in loose formation. SOLARA's objective is to demonstrate low-frequency interferometry in the range of 0.1 to 30 MHz. This frequency range spans the ionospheric cut-off (~10MHz, depending on conditions) and allows some overlap with established ground-based observatories (LOFAR, LWA) to aid in calibration.

As described in Section II, SOLARA is intended to be a starting point for a larger interferometer capable of exoplanet observations. However, the number of spacecraft that comprise SOLARA is sufficient for SOLARA to function as a first-class science instrument for solar, planetary, and galactic observations.

IV. SCIENCE REQUIREMENTS

The key metrics for any interferometer are angular resolution, sensitivity, frequency (or spectral) resolution, time resolution, and dynamic range. The properties of an astronomical object will set the values for the above parameters, so an observer must choose an observatory that suits the object they intend to observe. Conversely, interferometers may be designed with particular observations in mind. This is the case with SOLARA. Table 1 below lists the science requirements for three classes of observations (galactic mapping, heliophysics, and solar system planets). The requirements for exoplanets are similar to those for solar system planets, but the sensitivity must be much higher. Exoplanetary signals are expected to be in the range of mJy – μJy [14], so 10^3 – 10^6 more sensitivity will be required for exoplanets than for Neptune.

Table 1 - Requirements for three SOLARA science cases.
A Jansky (Jy) is 10^{-26} W/m^2/s/Hz. See Section IV.II for a detailed discussion of acceptable orbits. The values in this table for acceptable orbit are based only on the local plasma frequency, not station-keeping considerations. The altitudes are minimum values, not necessarily desired values.

	Galactic Mapping	**Solar bursts**	**Solar System Planets**
Sensitivity	10^6 – 10^7 (Jy/sr) <10,000 K	10^6 Jy	25,000+ Jy (Jupiter) – 1 Jy (Neptune)
Dynamic range	1000 (30 dB)	20 – 30 dB	20 – 30 dB (or greater)
Frequency range	1 MHz – 50 MHz (to overlap w/	100 kHz (1/2 AU) – 30 MHz +	100 kHz – 40 MHz +

	ground)		
Acceptable orbit	High LEO **(> 500 km**, above e^- density peak)	Near or above plasmapause (4-6 R_{Earth}, **25,000 – 38,000 km** +)	Near or above plasmapause (4-6 R_{Earth}, **25,000 – 38,000 km** +)
Resolution (spatial)	~1°	~1°	<1° (< 1' preferred)
Resolution (time)	N/A	Minutes	Seconds - hours
Required observation duration/mission lifetime	Days – weeks (months for improved sensitivity)	Months (collect statistics on multiple bursts/CMEs)	Months (to see variations due to solar wind conditions)

SOLARA's design is tailored primarily to the requirements for galactic mapping and solar bursts with observations of solar system planets (particularly Jupiter and Saturn) as stretch goals. Refinement of the SOLARA science and technical requirements is an ongoing task.

V. INTERFEROMETRY WITH SOLARA

Observational astronomy is driven by the fundamental $\theta = \lambda/D$ relationship between the observed wavelength (λ), aperture diameter (D), and angular resolution (θ, in radians). Observations at longer wavelengths require correspondingly larger apertures in order to obtain reasonable angular resolution. When λ/D is less than ~1/10, a parabolic reflector provides essentially no angular resolution. The Arecibo telescope (D = 300 m) is close to the practical limit for monolithic parabolic reflectors, but is of little use for 30 MHz observations (λ = 10 m).

Interferometry provides an alternative to building ever-larger monolithic parabolic apertures to improve angular resolution. Using multiple small apertures (either parabolic or dipolar) spread over a large area, it is possible to construct a sparse aperture with an effective diameter (D) that is equal to the maximum spacing (baseline B) between elements. The signals from each element of the interferometer must be appropriately delayed (phased) and then cross-correlated in order to measure astronomical signals from a particular direction. This technique allows effective areas ranging from 10s to 100s of kilometers up to the full diameter of the Earth with Very Long Baseline Interferometry (VLBI).

An interferometer requires accurate knowledge of the location of each element so appropriate phase delays can be applied. In radio interferometry, these delays are either applied mathematically after digitization or by the use of physical delay lines which increase the signal travel time to the correlator. Synchronized and accurate clocks/oscillators at each receiver are also required to reduce phase errors.

The aperture plane of an interferometer is defined by a projection of the baseline vectors between each pair of antennas. This collection of vector endpoints is known as the UV plane. The U axis traditionally points east, V points north, and the normal vector of the UV plane points toward the phase center of the array (typically the location of the observation target). See Figure 2. The number of unique baselines in an interferometer is n(n-1)/2 where n is the number of antennas.

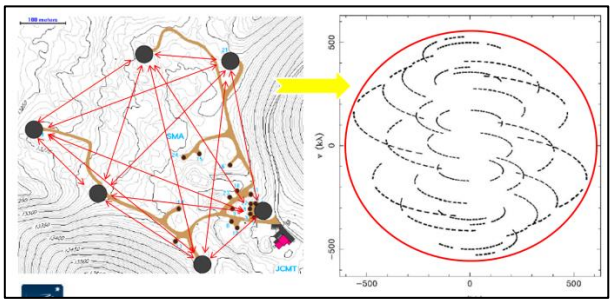

Figure 2 - Physical baselines (left) to UV plane (right).

The left panel shows the baseline vectors between the antennas of the SubMillimeter Array (SMA). The antennas are black circles and the baselines are represented by red arrows. The right panel shows the uv coordinates for the physical baselines accumulated over time as the Earth turns relative to the observatory. The Earth's motion changes the projection of the baseline vectors as a function of time and therefore changes the uv coordinates corresponding to a single baseline. The UV plane filling can be improved (with a corresponding improvement in

image quality) by allowing significant Earth rotation. This technique is known as Earth Rotation Synthesis. The outer red circle overlaid on the UV plane represents the effective aperture (D) for the interferometer. Image adapted from NRAO Synthesis Imaging Workshop 2014, credit: David Wilner.

IV.I. Metrology Requirements

The requirement for baseline measurement precision scales with the observed wavelength. To avoid large phase errors, the baseline length and orientation should be known to 1/10 – 1/16 of a wavelength. For this reason, optical interferometry is extremely difficult as it requires baseline knowledge (and often control) to the nm level while radio interferometry is comparatively easy. For $\lambda = 10$ m (30 MHz), baseline knowledge of 1 m is sufficient.

Baselines will be measured via two-way ranging at a higher frequency than the observation frequency range (likely S-band or X-band). The measurement accuracy and precision will be a direct function of the stability and synchronization of the onboard clocks on each spacecraft. The details of the error budget and the contribution of clock drift and temperature dependence will be the subject of a future paper.

Another key question is whether the baselines must be *controlled* to 1 m precision, or whether baseline *measurement* is sufficient. If constant control is required, the spacecraft and constellation design become significantly more exacting. For SOLARA, we have chosen to avoid the problem of tight formation control by allowing the spacecraft to drift relative to one another. In this scenario, the maximum integration time for an observation is set by the amount of time that it takes for baselines to drift 1/10 of a wavelength (at which time another baseline measurement must be taken before the next integration).

IV.II. Constellation Orbit

The choice of orbital location is critical for the success of SOLARA. The three critical factors are:

1. Free electron number density in the direction of observation
2. Strength of orbit perturbations
3. Distance (for communication to Earth, RFI mitigation)

The first criterion is directly related to SOLARA's science requirements (see Table 1), while the second and third criteria are primarily related to engineering considerations like propellant budget and sizing of the communication system.

Electromagnetic waves cannot propagate through plasma when the frequency of the EM wave is equal to or less than the plasma frequency. The plasma frequency can be approximated as $\nu_p \sim 9*(N_e)^{1/2}$, where ν_p is the plasma frequency in kHz and N_e is the number density of electrons per cm^3. Figure 3 shows the electron number density as a function of radial distance from the Earth and the corresponding plasma frequencies. Low Earth Orbits (LEOs) are not feasible for SOLARA because the local plasma frequency is too high and orbit perturbations will be strong, causing rapid constellation drift. GEO is a better option (and may be ideal for a precursor demonstration, but is likely too crowded for the full constellation. Higher and/or non-geocentric orbits are acceptable in terms of electron density. The solar wind electron density (

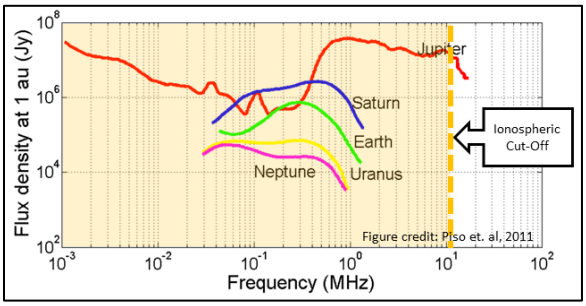

Figure 1, top) is the lower limit for orbits around 1 AU. Of course, spacecraft in distant orbits will also require additional radiation shielding/hardening.

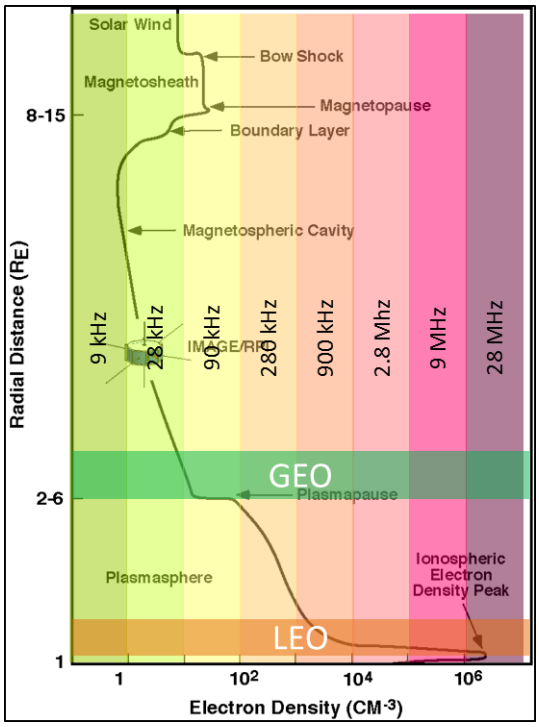

Figure 3 - Electron density as a function of radial distance from Earth.

The black curve traces the electron density at increasing distance from the Earth (measured in Earth radii). The vertical color bars represent decades of electron density (and corresponding plasma frequency) increasing from left to right. The locations of Low Earth Orbits (LEO) and Geostationary Orbits (GEO) are shown as orange and green horizontal bars respectively. The plasma frequency represents the absolute lower limit for observations. In practice, observing near the local plasma frequency will introduce significant distortions from scattering and refraction. Original figure from Green, et. al. (1995) http://image.gsfc.nasa.gov/publication/document/1997_green_etal/

To satisfy the second and third criteria, a dynamically quiet orbit not too far from Earth is ideal. In Section IV.IV, a detailed analysis of one such orbit, a lunar L1 (LL1) halo orbit, is presented. Similar work on lunar L4/L5 orbits is underway currently. A distant retrograde orbit (DRO) has been suggested for reduced station-keeping [1], [2], [15]. Despite the opacity of the ionosphere to low-frequency manmade radio noise, some does leak out through ducts in the ionosphere. For this reason, the lunar farside (either on the surface or in an orbit where the Earth is eclipsed by the moon) is considered optimal for very high sensitivity observations [16], [17]. This shielding effect was observed directly by RAE-2 [18]. Due to the fairly "lumpy" gravity field of the moon [19], however, lunar orbits require significant station-keeping. Lunar orbits were not considered for SOLARA. While an LL1 orbit was considered, and LL2 orbit was not considered because of the increased distance to Earth and concomitant decrease in communication bandwidth (as well as periodic blackouts due to the moon occulting the Earth).

IV.III. Constellation Architecture

SOLARA is an interferometer, so the constellation/formation is collectively a scientific instrument. Individual SOLARA spacecraft on their own are not particularly useful for collecting scientific data. Careful design of the constellation is therefore critical to the success of the mission. Three constellation architectures suggest themselves: all identical units ("peer-to-peer"), a single mothership and many less capable identical units ("single master"), or a hybrid of the first two ("hierarchical"). See [20] for a detailed network communication analysis of each case, taking failures into account.

The "peer-to-peer" architecture is the simplest from a spacecraft manufacturing and launch perspective. All spacecraft are identical and have equivalent performance. This architecture would leverage mass production techniques to reduce cost per unit. Effective networking among the units is critical for optimal performance, but this architecture is very robust to failure. For shared tasks (e.g. correlation), the loss of a constellation member would add only a small additional burden to the other spacecraft. Each member of the constellation, however, would need relatively large computing power in order to perform signal processing, network communication and data exchange, and correlation. This architecture would also imply a relatively low data rate to Earth if each spacecraft must communicate separately, or a fairly sophisticated arraying system for phased array communication to Earth (see [4] for detailed description of the SARA concept for phased array communication from a CubeSat constellation).

An alternative architecture is a single mothership with a swarm of smaller, less capable units that are the receivers for the interferometer. This is similar to how most ground-based interferometers

work, with the central correlator playing the role of mothership. The mothership, which might be the deployer of the smaller "slave" units, would be a larger small sat with more power generation, computational power, and communication bandwidth than the slaves. The slaves would collect data and then send it to the mothership for correlation and transmission to Earth. Constellation maintenance algorithms would run on the mothership and thrust commands would be transmitted to the slaves as needed. The highly capable mothership provides many advantages, but it is also a single point of failure. If the mothership fails and cannot be recovered, the constellation cannot function as an interferometer.

The third architecture is a hybrid of the "peer-to-peer" and "single master" approaches. Instead of a single mothership, there would be several (perhaps 3-4) slightly larger, more capable small sats along with a larger number of "slave" units to increase the number of baselines. The additional "masters" provide redundancy and robustness that the single mothership architecture lacks – there is no single point of failure. The smaller motherships can divide up the computational and communication burden and therefore could be smaller (perhaps still within the CubeSat size range). This approach is most robust for communications [20], but the "peer-to-peer" approach is preferred for simplicity of spacecraft design. The single mothership approach is likely only feasible and beneficial if a separate deployer spacecraft [21] is needed and must be included in any case.

IV.IV. LL1 Simulation and Beam Analysis

A simulation of a CubeSat constellation in a halo orbit around LL1 was developed by Kevin Gomez and Dr. Charles Lee [22]. This numerical simulation of the Circular Restricted 3-Body Problem (CR3BP) traced one halo orbit of each of the 20 bodies in a Y-formation (only 16 of the original 20 were used in the following analysis). See Figure 4.

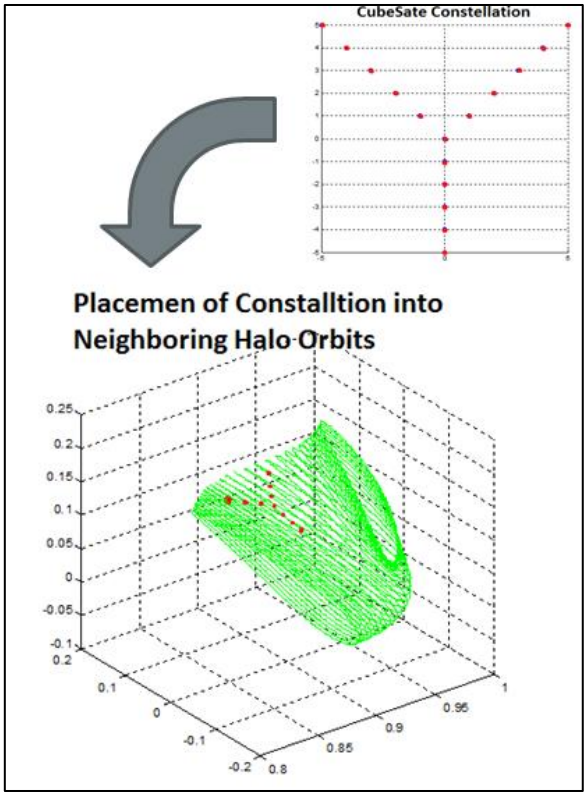

Figure 4 - Y-formation placed on halo orbits about LL1.
The green curves on the bottom panel represent paths along the stable manifold. The red dots are the starting positions of the CubeSats. Image credit: Kevin Gomez [22].

The output of the CR3BP numerical simulation was a state vector with (x, y, z) coordinates for each spacecraft at each time step in the simulation. The simulation lasted for approximately 11 days – roughly one period of the halo orbit. The state vector coordinates are in the rotating frame of the Earth-Moon system (Figure 5, top panel).

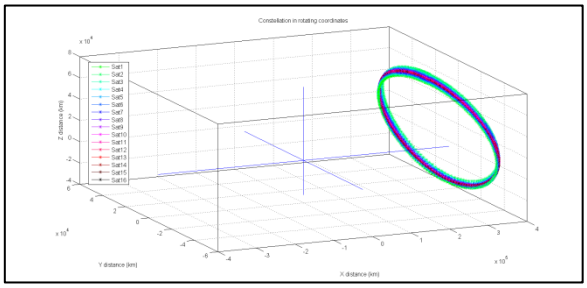

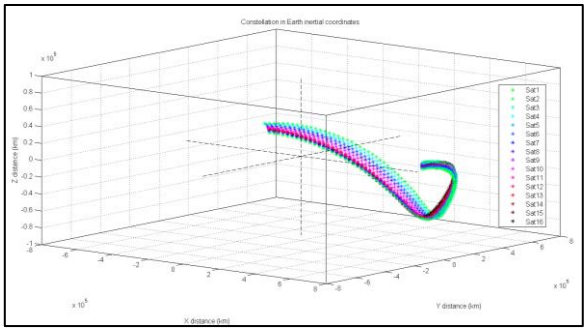

Figure 5 - LL1 constellation in rotating coordinates (top) and inertial coordinates (bottom).

The origin of the rotating coordinate system (top panel) is the LL1 point. The x-axis points toward the moon and the z-axis points north. In the rotating coordinate frame, the circular halo orbit is obvious. The circular structure disappears in the inertial Earth-centered coordinate system (bottom). The different colored points represent the positions of each spacecraft at each time step of the simulation.

The state vector from the CR3BP became input for a simulation of the interferometer beam (see Figure 6 for workflow). The input state vector was first transformed into an Earth-centered inertial frame. Then baseline vectors were calculated by simple vector subtraction for each spacecraft pair at each time step. Next, (u, v, w) coordinates were calculated from each baseline vector (B_x, B_y, B_z) via a matrix multiplication (representing a projection operation.

$$\begin{bmatrix} u \\ v \\ w \end{bmatrix} = \begin{bmatrix} \sin H & \cos H & 0 \\ -\sin H \cos H & \sin \delta \sin H & \cos \delta \\ \cos \delta \cos H & -\cos \delta \sin H & \sin \delta \end{bmatrix} \begin{bmatrix} B_x \\ B_y \\ B_z \end{bmatrix}$$

In the transformation matrix above, which was developed for arrays fixed to the Earth's surface, H represents the Hour Angle (HA) or azimuthal coordinate of a source. HA is used to take into account the rotation of the Earth, but in inertial coordinates right ascension (RA) can be substituted for HA. Declination (δ), the elevation or latitude coordinate, is the same in both the Earth inertial and rotating Earth systems. The (RA, δ) coordinates in the transformation matrix are where the phase center of the interferometer lies in celestial coordinates. In other words, the w-axis or normal to the UV plane points toward (RA, δ). The synthesized interferometer beam is centered on (RA, δ).

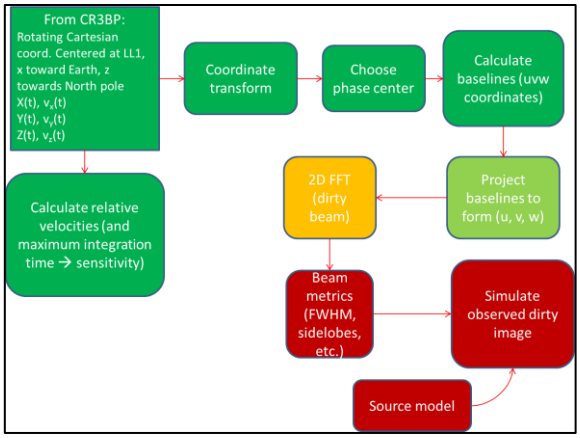

Figure 6 - Workflow from output of CR3BP to sky resolution map.

Green boxes are completed, yellow are in progress, and red are future work.

As described in Section V, the UV plane is essentially the aperture plane for an interferometer. For ground-based interferometers, the baseline vectors are typically very close to 2D rather than 3D, therefore the w-component of the (u, v, w) coordinate can safely be ignored. This is emphatically not the case for a space-based array except in the special case where the phase center is perpendicular to the surface of the stable manifold on which the stable halo orbits live. In the 2D case, there is a straightforward Fourier relationship between the sky brightness I(RA, δ) and the measured visibilities in the UV plane V(u, v). In the 3D case, one can formulate a 3D Fourier transform that includes the w-term, but performing a 3D Fourier transform multiple times as is required for interferometric image deconvolution would be extremely computationally intensive. There are approximations that are used in large ground-based interferometers (LOFAR, VLBI) that account for the w-term by using many "facets" within which the w-term can safely be projected away. It is likely these methods could be applied the inherently 3D space-based array, but further work is required in this area. For the purposes of the resolution simulation discussed here, the phase center was simply moved over a uniformly spaced grid of (RA, δ) rather than attempting to deal with the w-term in a wide-field imaging sense. Properly accounting for the w-term in imaging simulation is a topic for future work.

At each time step in the simulation, the set of baseline vectors was converted to (u, v, w) coordinates. This procedure was done for a set of

phase centers (RA, δ) which covered the full celestial sphere evenly in both RA and declination. Two examples spanning the full simulation time are shown in Figure 7. For each set of (u, v, w) coordinates for each time step and gridpoint, the maximum baseline was chosen and was used to estimate the full-width half maximum (FWHM) of the synthesized interferometer beam using the simple $\theta = \lambda/D$ relation. Each (RA, δ) gridpoint was assigned a resolution in arcseconds based on this calculation. A timeseries of full-sky resolution maps was produced by iterating over the full set of time steps. As the constellation moves in its halo orbit and the baseline vectors between spacecraft change with time, different parts of the sky can be imaged at different resolutions.

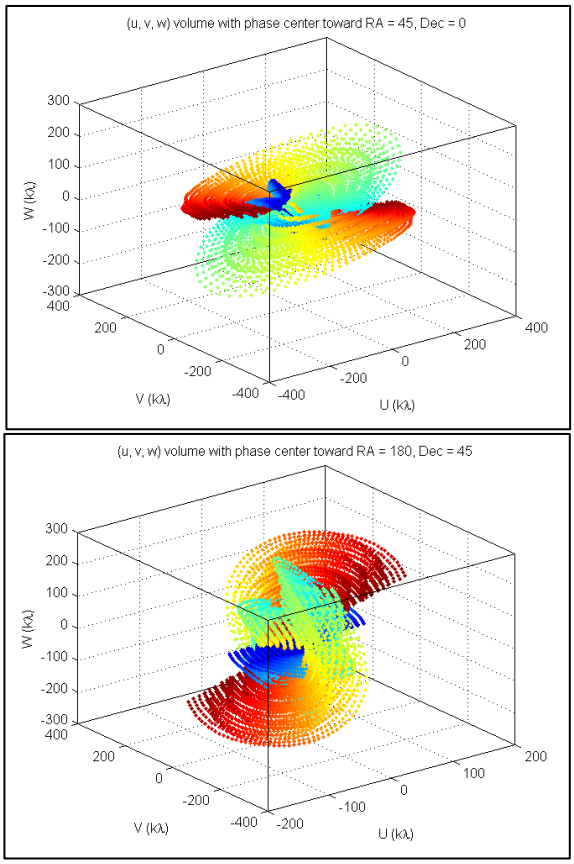

Figure 7 - (U, V, W) coordinates for two different phase centers.

The top panel represents a phase center of (45, 0) and the bottom panel is phased up toward (180, 45). The (u, v, w) points from each time step are plotted in the same color and the colors progress from blue to red from the beginning to the end of the simulation (exhibiting a type of "rotation synthesis"). Two features are striking – the w-term is of the same order as the u and v terms, and the shape of the (u, v, w) set changes markedly for different phase centers.

The conclusion that can be drawn from the timeseries resolution map (Figure 8) is that an LL1 constellation is not ideal for all-sky mapping. All-sky mapping requires consistent resolution elements across the full range of RA and declination. Given a sufficiently long observation time, the LL1 constellation might be able to produce such a map, but orbits with less relative motion between spacecraft would be preferable. On the other hand, the rapidly shifting resolution could be useful for imaging phenomena that occur on many spatial scales, such as solar bursts. The Y-configuration LL1 simulation is the starting point for examining constellations in different spatial arrangements at LL1 as well as constellation ins different orbits, particularly LL4/LL5 (discussed in the final section of this work).

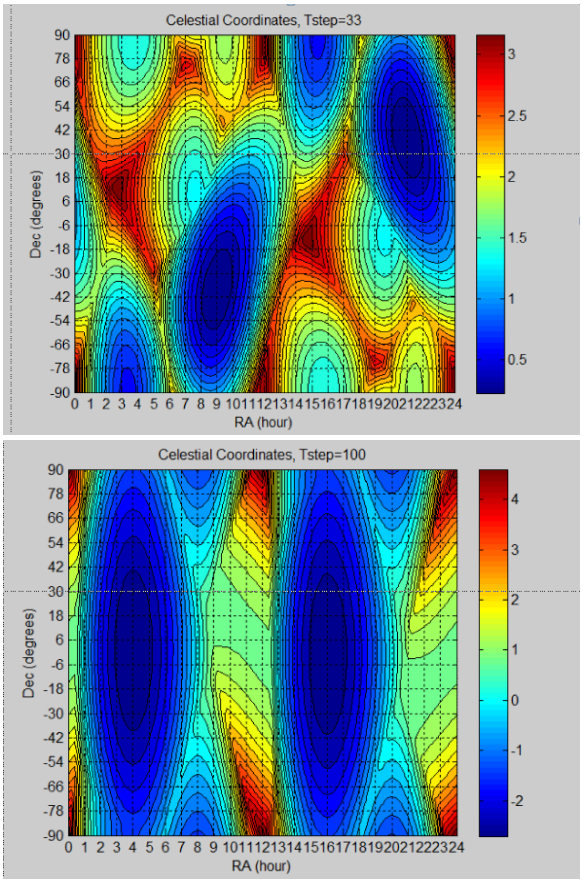

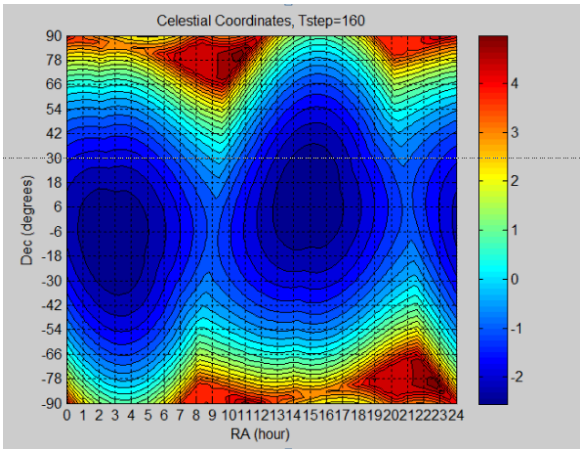

Figure 8 - Snapshots of angular resolution as a function of RA and declination.
The top panel is from t = 33, the second is t = 100, and the third is t = 160. The values of t are simulation time steps (min = 0, max = 215). The colorbar on the right represents angular resolution in arcseconds. Smaller numbers (shaded blue) are preferred for point source imaging. The vertical axis is declination in degrees and the horizontal axis is RA in hours (1 hour = 15 degrees).

In addition to generating a resolution map, relative velocities between pairs of spacecraft could be trivially calculated from the simulation output. The maximum and average values of relative velocity are shown in Figure 9. The maximum allowable relative velocities for a range of integration times are shown in Figure 10. Based on the observed relative velocities from this simulation, only integration times less than 1 second are practical. This is acceptable for bright sources like the sun, but impractical for faint sources which will not rise above the noise floor in a 1 second integration. The high relative velocities observed are another argument for choosing a different, quieter orbit with less relative motion.

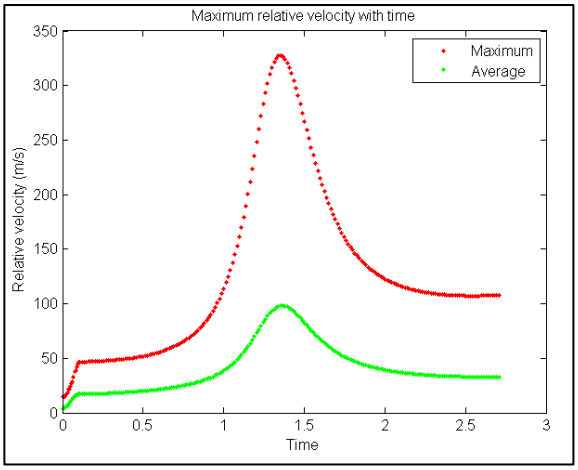

Figure 9 - Relative velocities throughout the simulation.
The red points are the maximum relative velocity experienced by any pair of spacecraft at each time point. The green points are the average of every spacecraft pair's relative velocity.

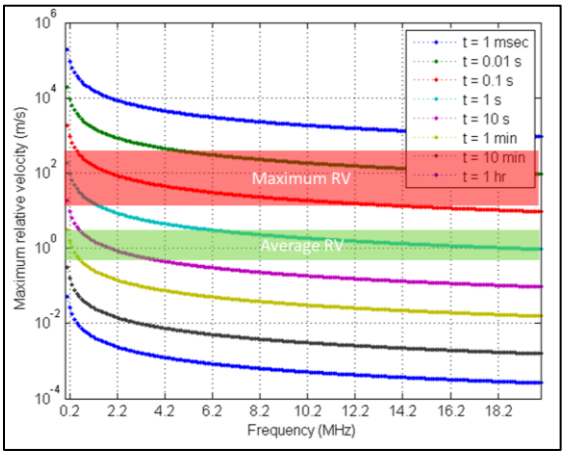

Figure 10 - Maximum allowable relative velocities.
The maximum permissible relative velocity between spacecraft is set by the distance the spacecraft move during one integration time relative to the wavelength being observed. Baselines must not change more than $1/10^{th}$ of a wavelength (preferable $1/16^{th}$ of a wavelength) during an integration to avoid large phase errors and corresponding source position errors. The colored curves represent different integration times starting with 1 msec at the top of the plot and moving down to 1 hour at the bottom of the plot. The red and green horizontal bars represent the range of velocities (maximum and average respectively) observed from the simulation data.

IV.V. Correlation

Raw voltage measurements from each SOLARA spacecraft must be properly delayed and cross-correlated in order to produce the set of complex visibilities that can be Fourier transformed into a map of the sky. Ground-based interferometers typically perform correlation at a central location using either customized hardware or efficient parallelized software (often GPUs). The sheer volume of data generated when Nyquist-sampling the antenna voltages on each spacecraft in several polarizations makes transmission of raw voltage data to Earth impractical. Space-based correlation is preferred so that the small correlated and averaged set of complex visibilities can be transmitted to the ground instead. The constellation architectures outlined in Section IV.III imply slightly different correlation schemes, but in all cases the correlation happens in space. From the perspective of ground-based correlation heritage, the single mothership architecture is the closest analog to existing systems. Correlation is an inherently parallel process, however, so it is well suited to distribution among many spacecraft. The raw voltage data would need to be transformed into the frequency domain and then each spacecraft would be responsible for correlating a small subsection of the total bandwidth [23]. Such a correlation scheme requires that each spacecraft is capable of performing relatively large FFT operations as well as reliably exchanging data with its fellows. Demonstrating such a system is a key task for precursor missions (Section VI).

V. SPACECRAFT DESIGN

This section presents a nominal design for each spacecraft subsystem (working under the "peer-to-peer" assumption that each spacecraft is identical). The subsystem designs presented intended to demonstrate that current (or near-future) technologies are available to meet the needs of a constellation like SOLARA. A lengthier, if dated, subsystem description is provided in [4]. Future systems engineering studies will be needed to refine the spacecraft design.

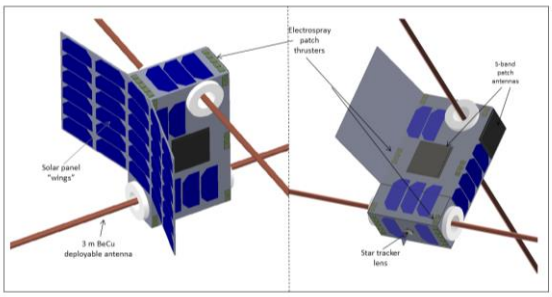

Figure 11 - Notional CAD model for a 6U SOLARA unit.

Radio Science Payload. The notional radio science payload consists of a set of electrically short crossed dipoles (perhaps STEM-type [24] deployables), a low-frequency optimized low-noise amplifier (LNA), and a low-frequency receiver. Radio receivers for SOLARA's range of frequencies have existed for many decades, so the challenge is in making the receiver small, radiation tolerant, and low power. Several groups have made progress in this area [25], [4]. A relatively large memory buffer will also be necessary to store measured voltages from the receiver until they can be correlated. The radio science payload will likely include one or more FPGAs for data processing. The choice of clock will be critical. The Chip-Scale Atomic Clock (CSAC) [26] appears to be an excellent option.

Communication. SOLARA CubeSats must be able to communicate amongst themselves as well as to the Earth. Intersatellite communication at S-band or perhaps X-band would permit a high data rate. There are existing S-band radios for CubeSats [27], and X-band radios are under development [28]. Data throughput optimization within the constellation network through the use of CDMA coding has been investigated [29]. In the "peer-to-peer" configuration (or hybrid configuration), the spacecraft could be phased up based on a control tone from the ground station and then transmit data in unison as a phased array to increase data downlink rate. See [4] for a more detailed explanation of this concept, developed by Alessandra Babuscia and named SARA for Separated Antennas Reconfigurable Array. In the case of a "mothership" , the larger spacecraft would carry a high-gain, high-power communication system that would handle all SOLARA-Earth traffic.

ADCS/Propulsion. The nominal design for the ADCS and propulsion system is the TSat system

[30]. This system consists of a modular set of small electrospray microthrusters which can be placed on the external surface of the spacecraft, an electronics stack to step up and regulate the voltage needed by the thrusters, and a set of HV cables to feed each thruster. An attitude sensing system based on sun sensors, gyros, and a magnetometer is currently being tested for TSat along with control algorithms tuned to the thruster actuators. For SOLARA, a star tracker would be added to the attitude sensor suite to move from degree-level attitude sensing toward arcsecond-level precision in both sensing and actuation. The antennas proposed are not particularly directional, but attitude knowledge on the same order as the desired angular resolution will be important for image deconvolution.

Power. A COTS power solution, including an EPS, batteries, and deployable solar panels is proposed. For a 6U bus, power generation of ~30 + W is expected. Since several vendors provide scalable CubeSat power systems, it is highly likely that a system can be chosen to meet power budget requirements with little customization. The placement of thrusters on the solar panels will, however, require a degree of customization and iteration with the manufacturer. This process will be investigated as part of the TSat precursor mission.

Avionics. As with the power system, the avionics hardware will be based on COTS products as much as possible. One (or more) FPGAs will likely be needed for processing radio science data, so it is possible that an FPGA-based flight controller architecture may be chosen. There is significant software development required for this system to function properly, but the goal of the precursor missions is to develop most of the critical software pieces and flight qualify them before attempting to implement SOLARA.

Structure. A 6U form factor has been chosen for each SOLARA unit as a baseline primarily to accommodate the STEM antenna deployment system. If that system could be miniaturized, a 3U form factor would suffice. A COTS structure is the most likely choice for the bus structure, although a custom structure is an option (particularly if the TSat unibody structure proves useful).

Thermal/Radiation. Any useful orbit for SOLARA will entail much higher radiation exposure than is typical for LEO CubeSats. Increased shielding, choosing radiation hard components, and software fault recovery will be critical to mission success. Radiation hard FPGAs are currently commercially available. The second precursor mission should provide some insight into the behavior of the components under high radiation dose. The thermal environments of the proposed orbits for SOLARA (and the second precursor mission) entail much more gradual thermal changes than LEO spacecraft experience (shorter or rare/nonexistent eclipses).

Delivery/deployment. One of the key benefits of CubeSat implementations is access to increasingly abundant launches as secondary/tertiary payloads. Most launches with CubeSat slots are to LEO or GTO. Launches that would provide access to lunar Lagrangian points or DROs are much less common. Some consideration was given to a potential delivery system in [4], where a modified ESPA ring with built-in propulsion and communication proposed as a delivery vehicle and potential mothership for the constellation.

An alternative to large vehicle delivery would be use of each individual CubeSat's propulsion system to travel from the drop-off orbit to the final constellation orbit. This would require a large portion of the propellant budget for transit and increases the risk of element losses while en route due to navigation or propulsion failures. The final choice of delivery/deployment strategy will depend on the evolution of the secondary payload launch environment as well as the availability (or lack thereof) of larger multi-CubeSat deployment vehicles capable of self-propulsion.

VI. PRECURSOR MISSIONS

Two precursor missions are proposed to smooth the way for the full SOLARA constellation of 16 spacecraft (which is itself a precursor for a more numerous and sensitive constellation). The first precursor mission, TSat, is currently under development at MIT [30]. Its purpose is to demonstrate an electric propulsion system capable of both attitude actuation and orbit maneuvers. Such a system will allow SOLARA spacecraft to perform orbit corrections as well as adjust attitude to maximize communication data rates.

The second precursor mission would involve 2-4 spacecraft in an Earth orbit to demonstrate baseline measurement, interferometry, intersatellite communication, distributed correlation, and perhaps formation control. These are the key capabilities that

SOLARA must have. The multi-spacecraft precursor mission is necessary to reduce the risk for these new CubeSat capabilities and improve the likelihood that a large space agency or firm will be willing to fund a large project like SOLARA. Earth orbit is problematic for low frequency radio interferometry due to ionospheric/magnetospheric plasma (Section IV.II), but there are many more launch opportunities to Earth orbit then Lagrange point orbits or DROs. An eccentric, inclined orbit (Molniya or HEO type) would be ideal because it allows the spacecraft a long period far from the Earth near apogee for observations, passes quickly through the radiation belts at high inclination, and passes close to the Earth at perigee for high communication bandwidth. While a minimum of two spacecraft can produce interferometric fringes, three spacecraft could achieve phase closure and four could achieve amplitude closure (in addition to adding baselines for improved image quality). A number larger than two would also be more relevant to demonstrating technologies necessary for management and control of larger constellations.

VII. FUTURE WORK

There are many research areas on the path to SOLARA and even larger constellations. The authors' future work will focus on simulating the science data products recovered from SOLARA observations given various error and noise sources. The location and distribution of the constellation is a key piece of this puzzle.

VII.I. Constellation control

The usual formation flight control problem consists of placing each spacecraft in its designated location and then strictly maintaining the relative positions of the formation members. The radio interferometry application suggests a different approach. Since variation in baseline magnitude and angle actually contributes to filling in the UV plane, a rigidly controlled constellation is not the optimal solution.

The relative locations of the spacecraft (as long as they can be measured) are not critically important. Instead, the properties of the constellation, such as distribution of baseline magnitude and angle, maximum/minimum baseline length, etc., are important for high quality imaging. For example, there is a maximum useful baseline [31] set by broadening/scattering along the line of sight to the target. Spacecraft drifting too far would exceed this maximum baseline and would need to be corralled back into the main body of the constellation. The constellation/formation control problem therefore becomes an optimization problem where the interferometer properties are optimized according to the current science observations while fuel use for position adjustments is minimized. This problem will be considered in the near future at MIT in collaboration with JPL.

VII.II. Alternative constellation locations/configurations

The detailed LL1 constellation study described above indicates that LL1 is not the ideal location for a constellation such as SOLARA. Too many limitations are imposed by the shifting resolution and high relative velocities. Changing the configuration of the constellation from the widely spaced Y-shape to a more randomized, tightly packed cluster on adjacent halo orbits may offer improvements (and is currently being studied). Orbits around unstable Lagrangian points (LL1,2,3) will always be constrained to a thin stable manifold, so angular resolution will vary greatly from phase centers perpendicular to the manifold surface (good resolution) to phase centers parallel to the surface (poor resolution).

Alternative constellation locations may remove some of the restrictions imposed by orbits about unstable points. Moving to the stable LL4/LL5 points should allow a more 3D constellation configuration and should reduce relative velocities (for careful orbit choices). There is little change in distance to Earth from LL1 halo orbits to LL4/5 orbits, so communication would not be significantly affected. DROs are "quieter" still in terms of station-keeping needs and disturbances, but they are typically much farther from the Earth (~10^6 km from the Earth). Nevertheless, this class of orbits is worth investigating because of the large propellant savings and associated increase in constellation lifetime.

The software developed to evaluate the LL1 constellation case will work equally well for the above alternative constellation configurations as well as precursor mission Earth orbits. Future publications will describe the results for these configurations.

ACKNOWLEDGEMENTS

The author would like to thank Alessandra Babuscia, Charles Lee, and Kar-Ming Cheung from JPL's division 332 for the opportunity to focus on the constellation analysis over the summer at sunny JPL. Thanks also to Daniel Winterhalter, Joe Lazio, and Walid Majid at JPL for helpful discussions on the topic of radio astronomy and interferometry. Thank you to the Keck Institute for Space Studies (KISS) workshop for inspiration and motivation to move forward on this project. Finally, thank you to Prof. Sara Seager for supporting this line of enquiry.

REFERENCES

[1] D. Jones, R. Allen, J. Basart, T. Bastian, B. Dennison, K. Dwarakanath, W. Ericksong, D. Finley, M. Kaiser, N. Kassim, T. Kuiperl, R. Macdowall, M. Mahoney, R. Perley, R. Preston, M. Reiner, P. O. Rodriguez, R. Stone, S. Unwin, K. O. Weiler, G. Woan, and R. Wool, "The Astronomical Low Frequency Array : Explorer Mission for Radio Astronomy A Proposed Explorer Mission for Radio Astronomy," in *Radio Astronomy at Long Wavelengths*, R. G. Stone, K. W. Weiler, M. L. Goldstein, and J.-L. Bougeret, Eds. American Geophysical Union, 2000, pp. 339–349.

[2] R. J. MacDowall, S. D. Bale, L. Demaio, N. Gopalswamy, D. L. Jones, M. L. Kaiser, J. C. Kasper, M. J. Reiner, and K. W. Weiler, "Solar Imaging Radio Array (SIRA): A multi-spacecraft mission," vol. 5659, no. May 2012, pp. 284–292, Jan. 2005.

[3] M. Bentum and A. J. Boonstra, "OLFAR - Orbiting Low Frequency Antenna for Radio Astronomy."

[4] M. Knapp, A. Babuscia, R. Jensen-clem, and F. Martel, "SOLARA / SARA : Solar Observing Low-frequency Array for Radio Astronomy / Separated Antennas Reconfigurable Array," in *Innovative Ideas for Micro/Nano-Satellite Missions*, R. Sandau, S. Nakasuka, R. Kawashima, and J. Sellers, Eds. International Academy of Astronautics (IAA), 2013, pp. 2–15.

[5] G. A. Dulk, Y. Leblanc, and T. S. Bastian, "Search for Cyclotron-maser Radio Emission from Extrasolar Planets," *Am. Astron. Soc.*, vol. 29, 1997.

[6] S. K. Sirothia, A. L. Etangs, and N. G. Kantharia, "Search for 150 MHz radio emission from extrasolar planets in the TIFR GMRT Sky Survey," vol. 108, pp. 1–9, 2014.

[7] T. S. Bastian, G. A. Dulk, and Y. Leblanc, "A Search for Radio Emission from Extrasolar Planets," *Astrophys. J.*, vol. 545, no. 2, pp. 1058–1063, Dec. 2000.

[8] A. Gurnett, "The Earth as a Radio Source: Terrestrial Kilometric Radiation," *J. Geophys. Res.*, vol. 79, no. 28, pp. 4227–4238, 1974.

[9] A. G. Smith and T. D. Carr, "Radio-Frequency Observations of the Planets in 1957-1958.," *Astrophys. J.*, vol. 130, p. 641, Sep. 1959.

[10] K. Ronald, D. C. Speirs, A. D. R. Phelps, and R. Bingham, "Analysis of a cyclotron maser instability with application to space and laboratory plasmas," *Proceedings of the 46th Annual Meeting of the Division of Plasma Physics*. 13-Jul-2005.

[11] M. D. Desch and M. L. Kaiser, "Predictions for Uranus from a radiometric Bode's law," *Nature*, vol. 310, no. 5980, pp. 755–757, Aug. 1984.

[12] J. N. Chengalur, Y. Gupta, and K. S. Dwarakanath, "Low Frequency Radio Astronomy — NCRA-TIFR," 2003. [Online]. Available: http://www.ncra.tifr.res.in/ncra/gmrt/gmrt-users/observing-help-for-gmrt-users/low-frequency-radio-astronomy/. [Accessed: 01-May-2014].

[13] P. Zarka and P. Z. Ã, "Plasma interactions of exoplanets with their parent star and associated radio emissions," *Planet. Space Sci.*, vol. 55, no. 5, pp. 598–617, Apr. 2007.

[14] J.-M. Grießmeier, P. Zarka, and H. Spreeuw, "Predicting low-frequency radio fluxes of known extrasolar planets," *Astron. Astrophys.*, vol. 475, no. 1, pp. 359–368, Nov. 2007.

[15] D. Oberoi and J.-L. Pinçon, "A new design for a very low frequency space borne radio interferometer," no. 1988, p. 17, Dec. 2003.

[16] P. Zarka, J.-L. Bougeret, C. Briand, B. Cecconi, H. Falcke, J. Girard, J.-M. Grießmeier, S. Hess, M. Klein-Wolt, A. Konovalenko, L. Lamy, D. Mimoun, and A. Aminaei, "Planetary and exoplanetary low frequency radio observations from the Moon," *Planet. Space Sci.*, vol. 74, no. 1, pp. 156–166, Dec. 2012.

[17] J. O. Burns, J. Lazio, S. Bale, J. Bowman, R. Bradley, C. Carilli, S. Furlanetto, G. Harker, A. Loeb, and J. Pritchard, "Probing the first stars and black holes in the early Universe

with the Dark Ages Radio Explorer (DARE),” *Adv. Sp. Res.*, vol. 49, no. 3, pp. 433–450, Feb. 2012.

[18] J. K. Alexander, M. L. Kaiser, J. C. Novaco, F. R. Grena, and R. R. Weber, “Scientific instrumentation of the Radio-Astronomy-Explorer-2 satellite,” *Astron. Astrophys.*, vol. 40, pp. 365–371, 1975.

[19] M. T. Zuber, D. E. Smith, M. M. Watkins, S. W. Asmar, A. S. Konopliv, F. G. Lemoine, H. J. Melosh, G. A. Neumann, R. J. Phillips, S. C. Solomon, M. A. Wieczorek, J. G. Williams, S. J. Goossens, G. Kruizinga, E. Mazarico, R. S. Park, and D.-N. Yuan, “Gravity field of the Moon from the Gravity Recovery and Interior Laboratory (GRAIL) mission.,” *Science*, vol. 339, no. 6120, pp. 668–71, Mar. 2013.

[20] J. Finn, A. Babuscia, C. Lee, and K.-M. Cheung, “A Concept for a Constellation of CubeSats at the Lunar Lagrangian Point 1 (LL1) for Radio Aperture Interferometry Measurements: Network Analysis and Simulation,” in *Interplanetary Small Satellite Conference*, 2014.

[21] V. Stamenković, D. Breuer, and T. Spohn, “Thermal and transport properties of mantle rock at high pressure: Applications to super-Earths,” *Icarus*, vol. 216, no. 2, pp. 572–596, Dec. 2011.

[22] K. Gomez, C. Lee, A. Babuscia, and K.-M. Cheung, “On the Formations of a CubeSat Constellation at the Earth-Moon L1 Libration Point,” in *Interplanetary Small Satellite Conference*, 2014.

[23] A. W. Gunst, L. B. Venema, and A. Bos, “Distributed Correlator for Space Applications,” no. April, pp. 28–30, 2008.

[24] “STEM ™ JIB ANTENNA.” .

[25] O. Thesis, “[OLFAR : DESIGN OF FREQUENCY RECEIVER],” 2010.

[26] W. D. Jones, “Chip-Scale Atomic Clock - IEEE Spectrum,” 2011. [Online]. Available: http://spectrum.ieee.org/semiconductors/devices/chipscale-atomic-clock. [Accessed: 02-Oct-2014].

[27] C. Communications, D. Signs, T. Low, L. Communication, S. Point-to-point, F. Repeater, and H. V. Option, “MHX2420 The MHX2420 is a 2 . 4 GHz Frequency Hopping Spread Spectrum Modem , which can be optimized for long distance communication over 30 miles (50km). MHX2420 radios offer the fastest communication over the longest distances,” pp. 2–3.

[28] E. Peragin, H. Diez, F. Darnon, D. Belot, J.-P. Millerioux, J.-L. Issler, T. Dehaene, Y. Richard, G. Guillois, F. Sépot, and D. Simon, *X Band Downlink for CubeSat*. 2012.

[29] A. Babuscia, C. Hung, D. Divsalar, and K.-M. Cheung, “Code division multiple access communications systems for CubeSats at Lunar Lagrangian L1,” in *2014 IEEE Aerospace Conference*, 2014, pp. 1–10.

[30] M. E. Knapp, M. Van de Loo, A. Krishnamurthy, and F. M. Hicks, “TSat: Demonstrating attitude control and orbit maneuvers with electrospray microthrusters,” in *65th International Astronautical Congress*, 2014.

[31] S. Jester and H. Falcke, “Science with a lunar low-frequency array: From the dark ages of the Universe to nearby exoplanets,” *New Astron. Rev.*, vol. 53, no. 1–2, pp. 1–26, May 2009.